NACA RM E54D20

NACA

RESEARCH MEMORANDUM

INVESTIGATION OF SEVERAL DOUBLE-RAMP SIDE INLETS

By Leonard E. Stitt and George A. Wise

Lewis Flight Propulsion Laboratory
Cleveland, Ohio

NATIONAL ADVISORY COMMITTEE
FOR AERONAUTICS

WASHINGTON
August 27, 1954
Declassified October 28, 1960

NATIONAL ADVISORY COMMITTEE FOR AERONAUTICS

RESEARCH MEMORANDUM

INVESTIGATION OF SEVERAL DOUBLE-RAMP SIDE INLETS

By Leonard E. Stitt and George A. Wise

SUMMARY

Several double-ramp inlets, utilizing a variable-angle second ramp, were mounted on the fuselage of a supersonic airplane having a twin-duct air intake system and investigated in the Lewis 8- by 6-foot supersonic tunnel at Mach numbers of 1.5, 1.8, and 2.0. With all the inlets, the boundary-layer air from the precompression ramp bridged across the leading edge of the variable ramp. Increasing the precompression ramp angle from 3° to 10° increased the over-all total-pressure recovery from 0.79 to 0.85 at a Mach number of 2.0, including a 4 percent loss ahead of the inlet due to the forebody. The stable operating range was very limited, and in the pulsing region it was observed that one duct carried most of the air flow. It was also found that subsonic diffuser performance was dependent on both inlet Mach number and initial rate of diffusion.

INTRODUCTION

When the speed range of a turbojet-powered aircraft extends to Mach 2.0, it becomes desirable to utilize a variable-geometry inlet system if optimum performance of the engine is required at all flight speeds. Therefore, a twin-duct side intake system utilizing several double-ramp inlets with a variable second ramp was investigated in the Lewis 8- by 6-foot supersonic tunnel. The internal and external performance of one of these inlets was reported in reference 1. The object of this investigation was to make a detailed study of the inlet performance and incorporate any indicated improvement. The investigation was conducted at free-stream Mach numbers of 1.5, 1.8, and 2.0 over a range of mass-flow ratio and angle of attack.

SYMBOLS

The following symbols are used in this report:

A	area
L	length of subsonic diffuser, 81.5 in.

M	Mach number
m_3/m_0	engine mass-flow ratio, $\frac{\text{engine mass flow}}{\rho_0 V_0 A_i}$
$(m_3/m_0)_{max}$	maximum mass-flow ratio, based on theoretical oblique shock system
P	total pressure
p	static pressure
V	velocity
T	total temperature
W	air flow, lb/sec
x	distance from cowl lip, model station 36
α	model angle of attack, deg
λ	variable-ramp angle with respect to fuselage center line, deg
ρ	mass density of air
δ	$P_3/2116$
θ	$T_3/519$

Subscripts:

max	maximum
x	conditions at x-distance from cowl lip
0	free stream
1	fuselage survey station, model station 31
2	diffuser-inlet survey station, model station 40
3	diffuser-exit survey station, model station 100

Pertinent Areas

A_i projected frontal area of both inlets: 0.342 sq ft for 3° precompression ramp inlets; 0.360 sq ft for 10° precompression ramp inlets

A_3 flow area at diffuser discharge, 0.457 sq ft

APPARATUS AND PROCEDURE

A photograph of the model used in this investigation is presented in figure 1. The side inlets were mounted on a 1/4-scale fuselage forebody of a supersonic airplane. The geometrically similar ducts joined into a common duct at a model station that corresponded to the engine compressor face in the prototype airplane.

The model was sting-mounted in the tunnel through a system of strain-gage balances. A shroud, which formed a continuation of the fuselage but was independent of it, was used to protect the various mechanisms at the rear of the model. It is seen in figure 1 as a dark extension of the fuselage. Also evident in figure 1 is one of two exhaust vents that were mounted on the shroud to lower the pressure at the base of the model and ensure choking at the mass-flow control plugs.

Figure 2 presents a schematic diagram of the model, including internal flow stations and representative model cross-sections. The nose of the model was canted down at an angle of 5°, and the inlets were canted down at an angle of 3°, both with respect to the fuselage center line. Pilot vision, rather than inlet performance, was the reason for the droop of the nose.

Photographs and details of the various inlet configurations are presented in figures 3 and 4. In general, the inlets had a fixed precompression ramp and a variable-angle second ramp. The second ramp was faired into the main duct by means of a plate that was hinged to the duct wall at its downstream end (fig. 4(d)). Moving the variable ramp, then, also varied the area distribution and diffusion rate in the initial portion of the subsonic diffuser. The resulting area distributions are shown in figure 5.

Specific inlet configurations will be designated by three symbols, such as 3-R-0. The first symbol (3 in the example) will denote the angle of the precompression ramp. The second symbol will designate whether the variable ramp was hinged at its leading edge (F) or at model station 37 (R). The third symbol will designate the thickness of the spacer under the rear plate at model station 51.1 (fig. 4(g)), which was used to vary the area distribution in the initial part of the subsonic diffuser.

Boundary-layer removal was accomplished by means of ram-type boundary-layer scoops located beneath the center portion of the inlet ramps as shown in figure 4(b). Part of the boundary-layer air was bled through ducts which changed smoothly from a rectangular cross section to a circular cross section and discharged the boundary-layer air at the model exit station in a direction parallel to the main duct. Mass flows were controlled by means of remotely operated plugs (fig. 2). The air in excess of that passing through the bleed ducts was diverted by wedges, as shown in figure 4(b).

A description of the model instrumentation and computation methods can be found in reference 1.

The investigation was conducted at free-stream Mach numbers of 1.5, 1.8, and 2.0, at various angles of attack. Reynolds number, based on length of fuselage ahead of the inlet, was approximately 13×10^6.

RESULTS AND DISCUSSION

Inlet 3-R-0. - The internal performance of inlet 3-R-0 with the variable-ramp angle set at 19° is presented in figure 6 at a free-stream Mach number of 2.0. Lines of constant corrected weight flow are indicated on the performance curves; a particular one, labeled "match line," corresponds to the corrected weight flow required at an altitude of 35,000 feet by the J67-W-1 engine, the engine for which the airplane was designed. Peak total-pressure recovery occurred at positive angle of attack because of the downward cant of the inlet and forebody. The nose of the forebody was alined with the flow at angle of attack $\alpha = 5^\circ$ and unpublished data, taken in a previous investigation, indicated that the inlet would be nearly alined with the local flow at $\alpha = 3.5^\circ$. These unpublished data also indicated that the Mach number ahead of the inlet was essentially free stream. The reduction in internal performance at zero angle of attack was probably due to the local flow angle over the sharp lip side fairings. A peak total-pressure recovery of 79 percent was obtained for this inlet at the minimum stable subcritical mass-flow ratio.

The experimental point of lowest mass-flow ratio on figure 6 and all succeeding figures was the minimum stable point obtained at each angle of attack. A stable subcritical mass-flow range of approximately $8\frac{1}{2}$ percent of maximum mass flow was obtained at $\alpha = 3.5^\circ$ including that portion of the curve in which pressure recovery decreased rapidly with an increase in mass-flow ratio (from $0.875 < m_3/m_0 < 0.91$). In this region, one duct operated subcritically while the other operated supercritically, as discussed in reference 1.

A breakdown of the total-pressure losses in the inlet system for a free-stream Mach number of 2.0, an angle of attack of 3.5°, and the variable-ramp angle set at 19° is also presented in figure 6. Estimated values of subsonic diffuser losses were calculated using an adaption of the method of reference 2. The 4 percent loss in total-pressure recovery ahead of the inlet $\Delta P_{0-1}/P_0$ was obtained from unpublished results of a previous investigation using the same forebody configuration. The breakdown of losses is presented only for that range of mass-flow ratios over which both ducts were operating subcritically. Figure 6 indicates that the measured inlet shock losses $\Delta P_{1-2}/P_0$ were 0.13 as compared with a theoretical value of 0.07, while the subsonic diffuser losses $\Delta P_{2-3}/P_0$ were about the magnitude predicted.

Contours of total-pressure recovery at the inlet station for inlet 3-R-0 with the variable-ramp angle set at 19° are presented in figure 7(a) for Mach number 2.0 and angle of attack of 3.5°. The contours of the right duct (fig. 7(a)) indicate two distinct regions of air flow; the total-pressure recovery of the region near the outboard cowl wall was of the order of magnitude that would result from normal shock recovery following a 3° precompression, and the total-pressure recovery at the center of the duct was somewhat higher than would be expected from the 3-shock configuration. These high recovery lobes (of the order of 95 percent) are believed to result from near-isentropic compression following the precompression ramp shock caused by the boundary-layer air which bridged across the leading edge of the variable ramp. This boundary-layer bridge caused the second oblique shock to originate at a point downstream of the variable-ramp leading edge, thus causing the low compression region near the outboard cowl wall. A low compression region, similar to that discussed for the right duct, existed over part of the left duct near the outboard cowl wall; and, in addition, a rather large boundary layer was evident on the ramp surface at the top of the duct. It is believed that this thick boundary layer resulted from separation caused by an unintended gap at the top portion of the variable-ramp leading edge. The regions of low total-pressure recovery in both ducts accounted for the difference between theoretical and experimental inlet shock losses presented in figure 6. It is evident from the breakdown of losses (fig. 6) that the most improvement in over-all performance could be made by decreasing the total-pressure losses between stations 1 and 2, the region of the inlet shocks.

Inlet 3-R-0 with boundary-layer bleed. - In order to increase the pressure recovery at station 2, inlet 3-R-0 (bleed off) was designed to eliminate the bridging of the boundary-layer air between the precompression and variable ramps and to locate the second oblique shock at the leading edge of the variable ramp. The leading edge of the variable ramp was raised 0.03 inch above the precompression ramp to scoop off the boundary-layer air which was then discharged back to the free stream

through vents, as seen in figure 3(a). The effect of the precompression ramp boundary-layer bleed on the inlet total-pressure recovery contours is presented in figure 7(b). This figure indicates that the thick boundary-layer region in the left duct was eliminated; however, the low compression regions are now more extensive near the outboard cowl walls of both ducts. The inlet shock losses $\Delta P_{1-2}/P_0$ with this inlet were slightly higher than those obtained with inlet 3-R-0 without boundary-layer bleed. The increase in total-pressure losses probably resulted from a reduction in total-pressure recovery at the center of both ducts resulting from the elimination of the near-isentropic compression caused by the boundary-layer air.

The low compression regions near the outboard cowl walls on the inlet contours indicate that only part of the free-stream air was compressed by the first oblique shock and the inlet terminal shock. This indicates that the second oblique shock still originated at a point downstream of the leading edge of the variable ramp, probably because part of the boundary-layer air still bridged across the variable-ramp leading edge. This bridging occurred in spite of the fact that the boundary layer on the variable ramp was thin, as implied in figure 7(b).

Inlet 10-R-0. - The precompression wedge angle was increased from 3° to 10° with the purpose of decreasing the strength of the second oblique shock, and thus decreasing the possibility of bridging across the leading edge of the variable ramp, and also of taking advantage of a potentially higher supersonic recovery. The height of the precompression ramp from the fuselage surface was decreased from 0.5 to 0.3 inch in the design of inlet 10-R-0 (fig. 4(f)), since previous measurements indicated that 0.3 inch was sufficient to remove all the boundary-layer air developed by the forebody ahead of the inlet. With this configuration for $M_0 = 2.0$ and the variable-ramp angle set at 19°, the second oblique shock fell quite far ahead of the cowl lip. Contours of total-pressure recovery at the inlet are presented in figure 7(c) for this configuration (10-R-0). A carborundum strip was installed on the leading edge of the precompression ramp of the left duct to trip the boundary layer and reduce the bridging across the variable-ramp leading edge. The inlet contours of the right duct indicate a pressure recovery close to that expected from shock losses, and the low compression region encountered with the 3° precompression ramp inlets (fig. 7(b)) was eliminated. The left duct contours indicate a thicker boundary layer than that obtained in the right duct, and from schlieren photographs (not presented) it was evident that this resulted from the presence of the carborundum strip. Removal of the carborundum strip would probably cause flow similar to that obtained in the right duct (fig. 7(c)) to occur in the left duct.

The internal performance of inlet 10-R-0 with the variable-ramp angle set at 19° is presented in figure 8 for free-stream Mach numbers of 2.0 and 1.8. For $M_0 = 2.0$ (fig. 8(a)), the performance curves

indicate an increase in peak total-pressure recovery of 4 percentage points over that obtained with inlet 3-R-0. This peak recovery was obtained at angles of attack of 3.5° to 5°, as before, with significant reductions in performance at angles of attack of -1.5° and 9°. For $M_0 = 2.0$, a maximum stable subcritical mass-flow range of approximately 11 percent of maximum mass flow was obtained at angles of attack of 3.5° and 5°, decreasing to no stability at -1.5°. The maximum mass-flow ratio obtained was approximately that expected from theory.

With the second oblique shock far ahead of the cowl lip at $M_0 = 2.0$, the inlet could not capture enough mass flow for efficient matching with the J67-W-1 engine at 35,000 feet. As indicated on figure 8(a) by the intersection of the match line with the performance curves, the inlet would be forced to operate in the supercritical region at a lower total-pressure recovery than that available from this configuration.

For $M_0 = 1.8$ (fig. 8(b)), the maximum total-pressure recovery was 89 percent at a subcritical mass-flow ratio, and the maximum stable subcritical mass-flow range was approximately $11\frac{1}{2}$ percent of maximum mass flow. The dashed line on figure 8(b) represents the performance of the inlet in the unstable mass-flow region. Matching of the inlet at $M_0 = 1.8$ to the J67-W-1 engine at 35,000 feet would again occur in the supercritical region because of the low maximum mass-flow ratio.

Inlet 10-F-0. - Because the matching mass-flow ratio of inlet 10-R-0 was too low for efficient operation, inlet 10-F-0 was designed. The leading edge of the variable ramp was positioned to cause the resulting oblique shock to lie just ahead of the cowl lip at $M_0 = 2.0$. The variable ramp was hinged at its leading edge to provide a more aerodynamically clean inlet than that using the rear hinge. With the rear hinge and resulting sliding leading edge of the variable ramp, the inlet system presented a step to the air flow at higher variable-ramp angles.

The internal performance of inlet 10-F-0 at $M_0 = 2.0$ presented in figure 9(a) indicates that the increase in matching mass-flow ratio for this inlet over inlet 10-R-0 enabled it to match the engine at a significantly higher pressure recovery. The increase in subcritical performance with inlet 10-F-0 over that obtained with inlet 10-R-0 indicates the advantage of using the front hinge instead of the rear hinge.

Inlets 10-F-1/4 and 10-F-1/2. - In order to increase the stable subcritical mass-flow range, two modifications of inlet 10-F-0 were investigated. On the basis of results presented in reference 3, the back plate of the variable ramp was raised 1/4 inch (inlet 10-F-1/4) and then 1/2 inch (inlet 10-F-1/2) at model station 51.1 (fig. 4(g)), to incorporate a more gradual change in area variation in the initial part of the subsonic diffuser.

The internal performance of these two inlets is also presented in figure 9 for free-stream Mach numbers of 2.0 and 1.5. The performance curves indicate an improvement in the subcritical pressure recovery with inlets 10-F-1/4 and 10-F-1/2 over that obtained with inlet 10-F-0. This increased subcritical performance probably resulted from more efficient subsonic diffusion in the case of inlets 10-F-1/4 and 10-F-1/2. However, no increase in stable mass-flow range was obtained, probably because the addition of the spacers did not result in an appreciable stabilizing length (figs. 5(b), (c) and (d)).

Because inlet 10-F-1/4 proved to be one of the better inlets, an extensive investigation was conducted to obtain its internal and external performance, the results of which have been presented in reference 1. Part of this performance has been repeated in figure 10 for comparison with the other inlets presented in this report. For $M_0 = 2.0$, figure 10 indicates a peak total-pressure recovery of 85 percent, including a 4 percent loss ahead of the inlet due to the forebody, as compared with 79 percent for inlet 3-R-0. A comparison of the breakdown of losses in figures 10 and 6 indicates a decrease of 4 percentage points in inlet shock losses with inlet 10-F-1/4 from that obtained with inlet 3-R-0. This decrease resulted from increasing the precompression ramp angle from 3° to 10°. The level of pressure recovery in the low compression region near the outboard cowl wall at air-flow station 2 for inlet 10-F-1/4, presented in contours in reference 1, was approximately 7 percentage points higher than the pressure recovery in the low compression region for inlet 3-R-0 (figs. 7(a) and 7(b)).

The internal performance and breakdown of total-pressure losses for inlet 10-F-1/4 are also presented in figure 10 for $M_0 = 1.8$ and 1.5. The curves indicate peak total-pressure recoveries of 89 percent and 93.5 percent for $M_0 = 1.8$ and 1.5, respectively.

It was also observed that for all the 10° precompression ramp inlets the boundary-layer air from the precompression ramp still bridged across the variable-ramp leading edge, as it did with the 3° precompression ramp inlets.

Performance in pulsing region. - Figure 11 presents the internal performance and diffuser-exit total-pressure recovery contours in the pulsing region for inlet 10-F-1/2 and a free-stream Mach number of 1.8. As the mass-flow ratio decreases and pulsing starts, the left duct carries most of the mass flow (fig. 12(a)). The left duct carries progressively more mass flow while the over-all pressure recovery decreases as the mass-flow ratio is further reduced (fig. 11(b)). Between points 11(b) and 11(c), the twin-duct flow pattern reverses and the right duct carries nearly all the flow (fig. 11(c)) with a slight increase in total-pressure recovery. When the mass-flow was increased from point 11(c),

the inlet performance followed the upper curve with the left duct carrying progressively more mass flow (fig. 11(d)). Pressure-sensitive pickups in each duct indicated that the twin ducts pulsed in phase at point (a). At point (b) the amplitude of the pulsation decreased and the pulsing became intermittent, but was still in phase. At point (c) the amplitude and frequency of the pulsation increased with no in-phase pulsing, and at point (d) the ducts pulsed as they did at point (b).

Detached wave performance. - Figure 12 presents the performance of inlet 10-R-0 at Mach number 1.5 with the variable-ramp angle set high enough to detach the second shock. A comparison of figure 12 for $\lambda = 20^\circ$ with figure 10(c) for $\lambda = 10^\circ$ indicates a reduction of only $1\frac{1}{2}$ percentage points in maximum total-pressure recovery from detaching the variable-ramp shock. It is also evident from figure 12 that with the reduction in maximum mass-flow available with detached wave operation, the inlet would be forced to match the engine in the far supercritical region. A comparison of the minimum stable mass-flow ratio points of figures 12 and 10(c) indicates that a lower air flow could be obtained with the inlet, before pulsing started, by detaching the variable-ramp shock. This conceivably could offer a method of obtaining lower inlet air flow for matching at reduced engine speeds without the danger of inlet instability. A comparison of the breakdown of total-pressure ratio losses in figures 12 and 10(c) indicates approximately the same supersonic recovery for the two conditions but a higher subsonic diffuser loss in the case of the detached wave, probably caused by the higher inlet Mach number.

Subsonic diffuser performance. - Figure 13 presents the subsonic diffuser performance for inlet 10-F-1/4 over the range of variable-ramp angles tested for several inlet Mach numbers. This Mach number, in all cases, was the value obtained at the inlet rake station, which was 4 inches downstream of the cowl lip. Figure 5(c) presents the change in diffuser area variation with changes in variable-ramp angle setting. The dashed lines on figure 13 represent the diffuser performance estimated by an adaptation of the method of reference 2. These estimated curves indicate an increase in diffuser efficiency with increasing initial rates of diffusion. The experimental results indicate a trend similar to the estimated curves up to a variable-ramp angle of approximately 13°. At angles greater than 13°, the diffuser efficiency decreased rather rapidly. The trend of the experimental curves was similar to that presented in reference 4; however, in reference 4 the diffuser efficiency peaked at a higher rate of expansion than it did in this investigation. It is also evident from both the estimated and experimental curves that diffuser efficiency decreased with increasing inlet Mach number for a given area distribution.

SUMMARY OF RESULTS

An investigation was conducted in the Lewis 8-by 6-foot supersonic wind tunnel to determine the performance characteristics of a twin-duct air-intake system utilizing several variable-geometry double-ramp inlets. The investigation was conducted at Mach numbers of 1.5, 1.8, and 2.0. The following results were obtained:

1. For all the double-ramp inlets investigated the boundary-layer air from the precompression ramp bridged across the leading edge of the variable ramp, causing the second oblique shock to originate at a point downstream of the variable-ramp leading edge. This, of course, would compromise any design based on a theoretical shock configuration.

2. Increasing the precompression ramp angle from 3° to 10° increased the over-all total-pressure recovery from 0.79 to 0.85 at a Mach number of 2.0, including a 4 percent loss ahead of the inlet due to the forebody, because of the lower inlet shock losses attendant with the higher ramp angle.

3. In the pulsing region dissimilar duct operation was obtained in that one duct carried most of the mass flow.

4. For a given inlet Mach number the subsonic diffuser efficiency was dependent on the initial rate of subsonic diffusion, and, for a given area distribution, the subsonic diffuser efficiency decreased as the inlet Mach number increased.

Lewis Flight Proplusion Laboratory
National Advisory Committee for Aeronautics
Cleveland, Ohio, April 22, 1954

REFERENCES

1. Obery, Leonard J., Stitt, Leonard E., and Wise, George A.: Evaluation at Supersonic Speeds of Twin-Duct Side-Intake System with Two-Dimensional Double-Shock Inlets. NACA RM E54C08, 1954.

2. Bailey, Neil P.: The Thermodynamics of Air at High Velocities. Jour. Aero. Sci., vol. 11, no. 3, July 1944, pp. 227-238.

3. Nettles, J. C.: The Effect of Initial Rate of Subsonic Diffusion on the Stable Subcritical Mass-Flow Range of a Conical Shock Diffuser. NACA RM E53E26, 1953.

4. Patterson, G. N.: Modern Diffuser Design. The Efficient Transformation of Kinetic Energy to Pressure. Aircraft Eng., vol. X, no. 115, Sept. 1938, pp. 267-273.

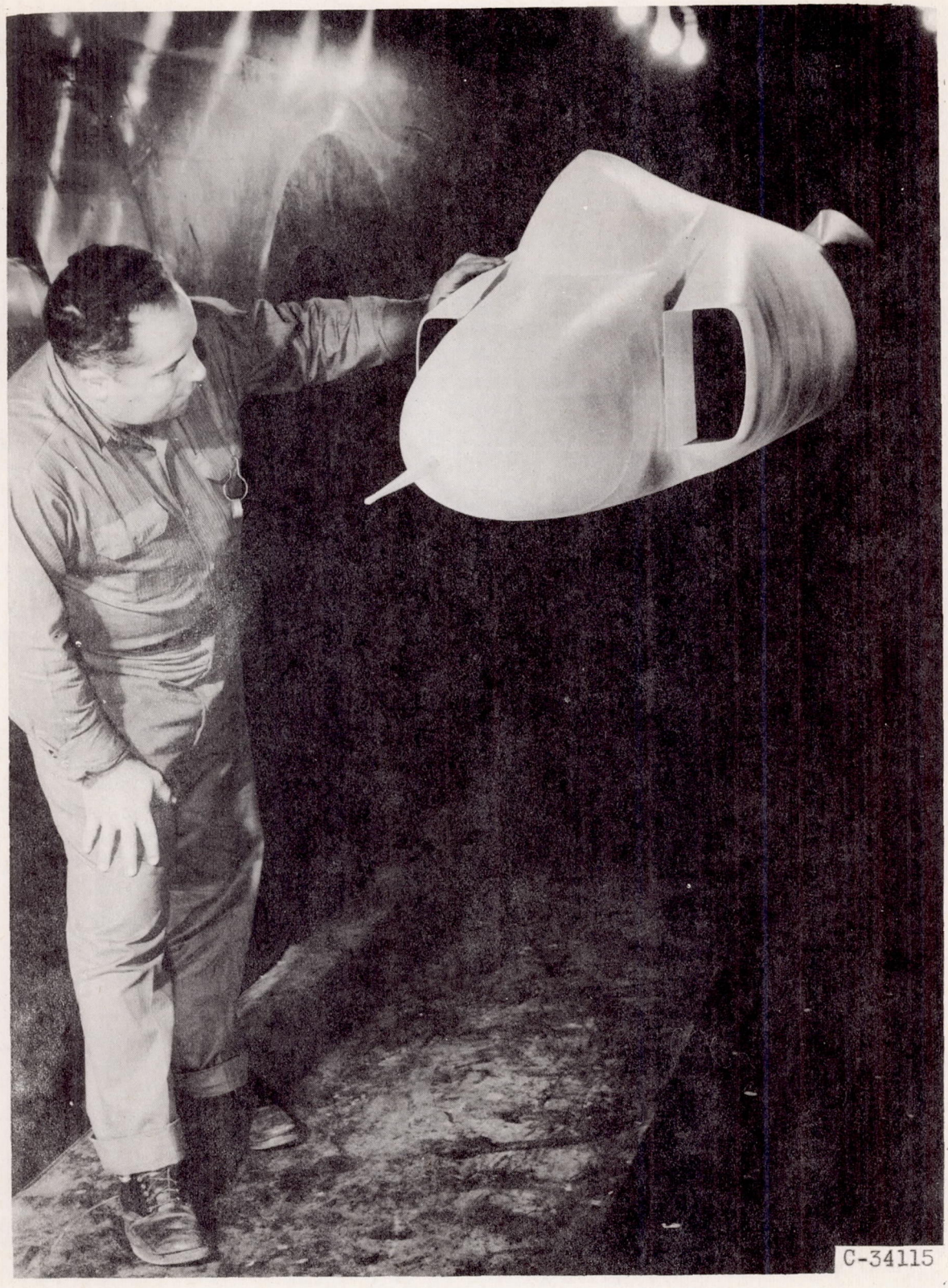

Figure 1. - Photograph of model in tunnel.

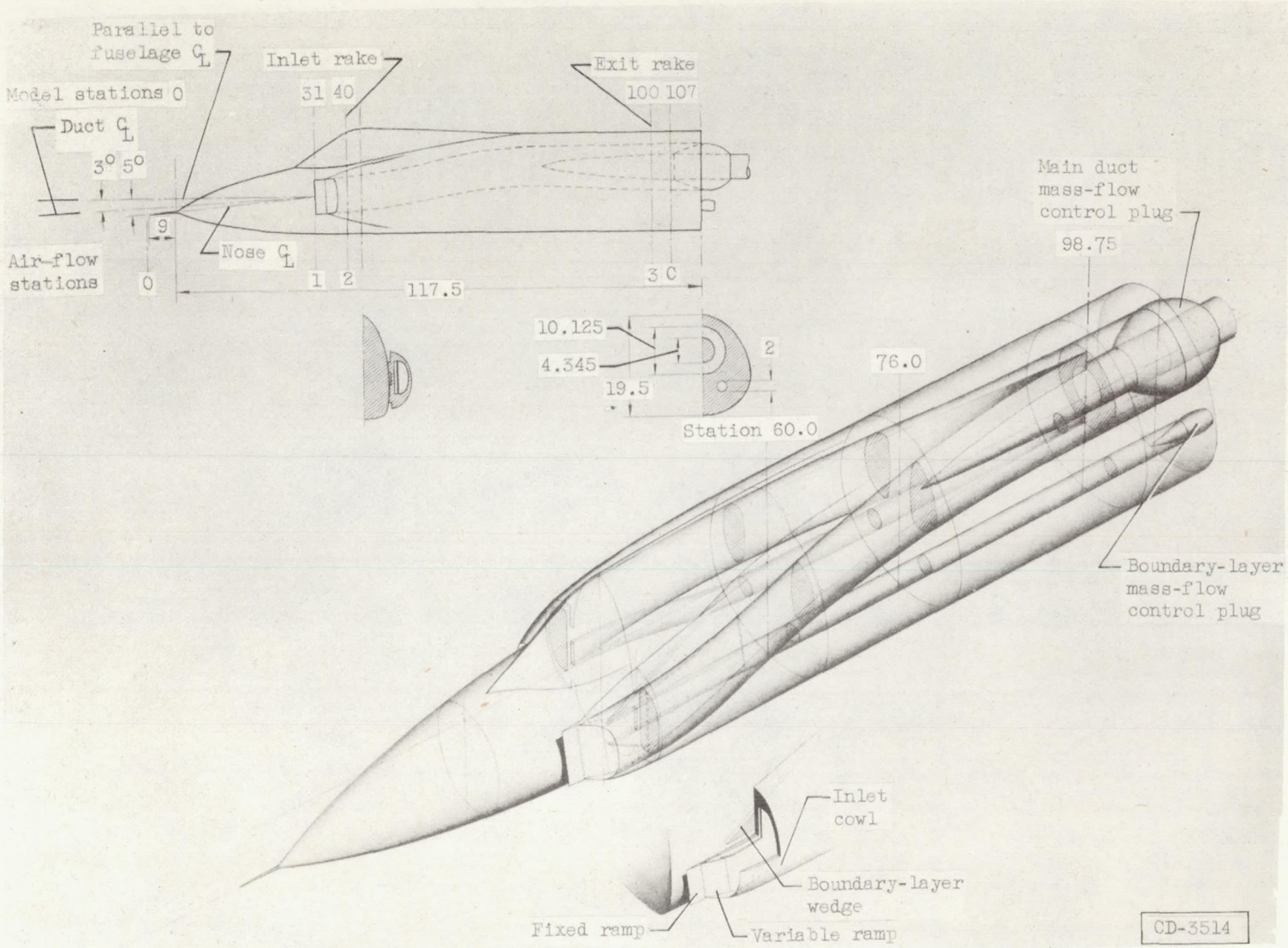

Figure 2. - Diagram of model with representative cross sections (all dimensions are in inches).

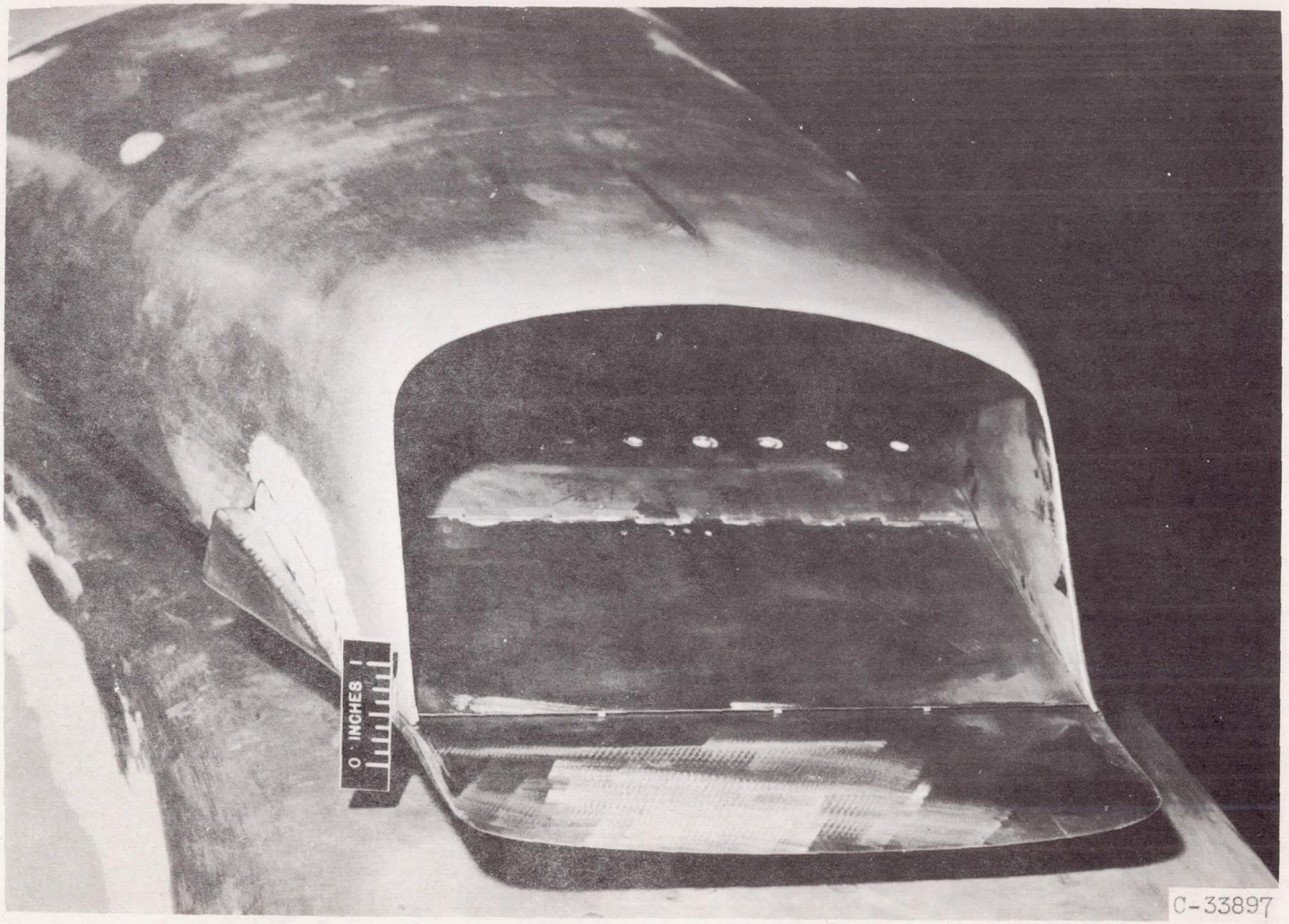

(a) Inlet 3-R-0 boundary-layer bleed.

Figure 3. - Photographs of inlets.

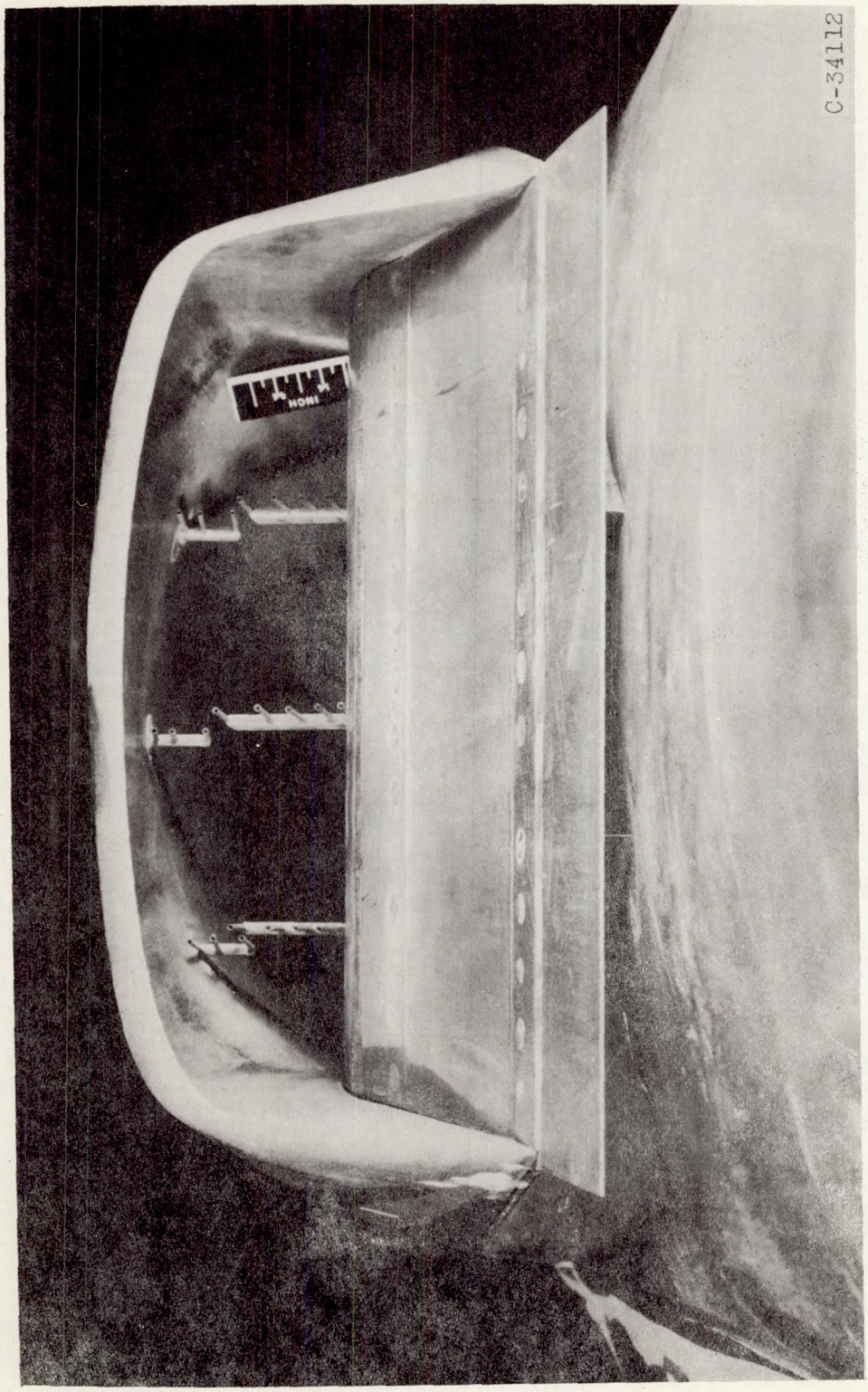

(b) Inlet 10-F-0.

Figure 3. - Concluded. Photographs of inlets.

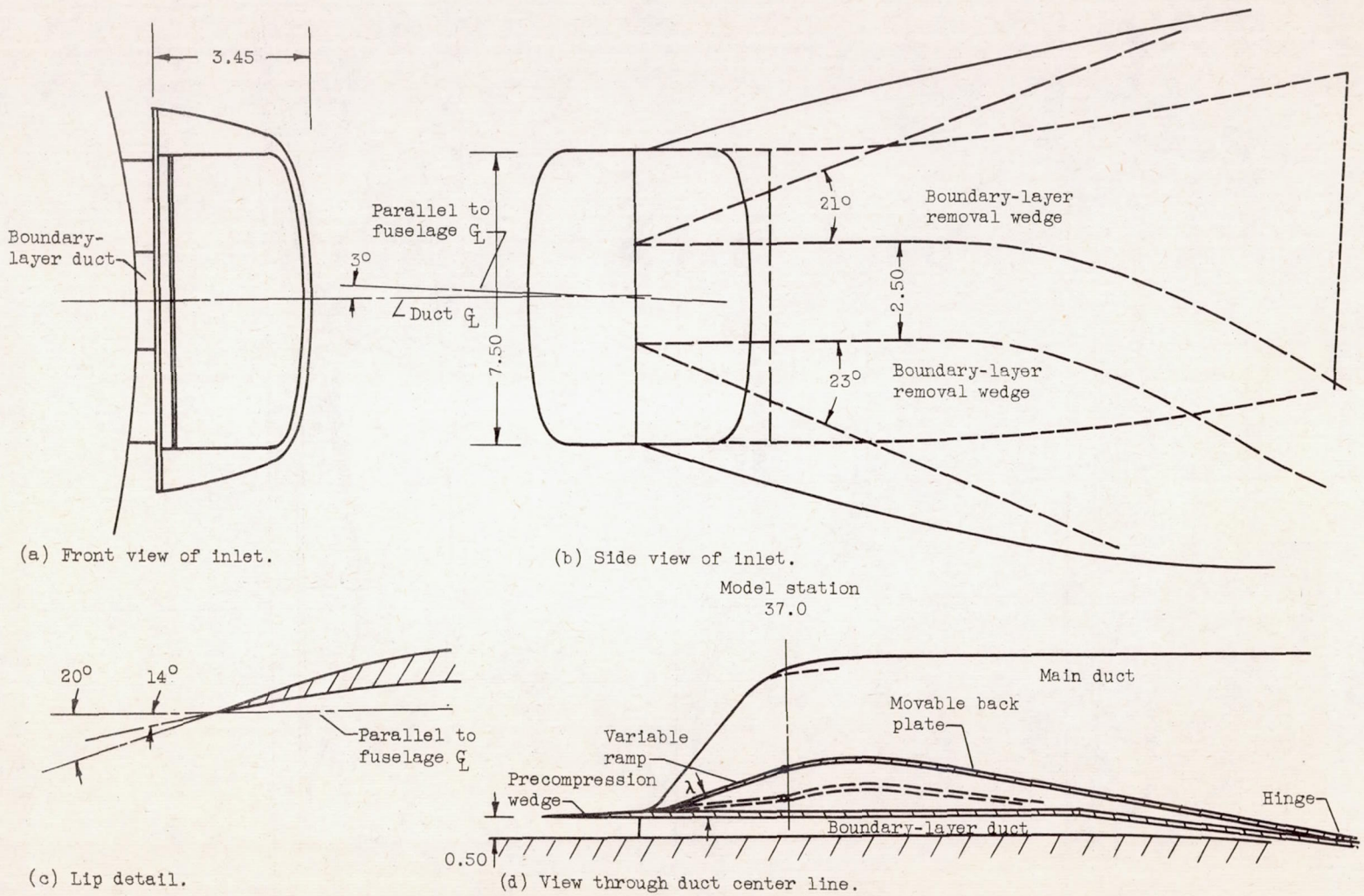

(a) Front view of inlet.

(b) Side view of inlet.

(c) Lip detail.

(d) View through duct center line.

Figure 4. - Detailed views of inlet configurations (all dimentions are in inches).

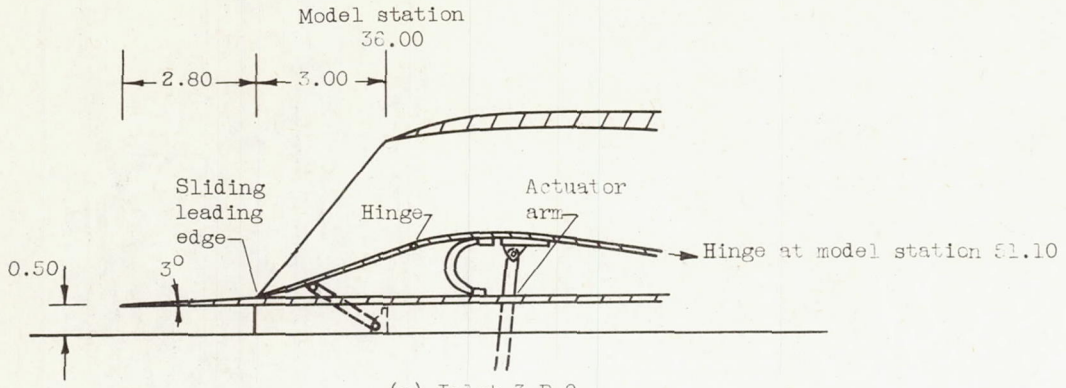

(e) Inlet 3-R-0.

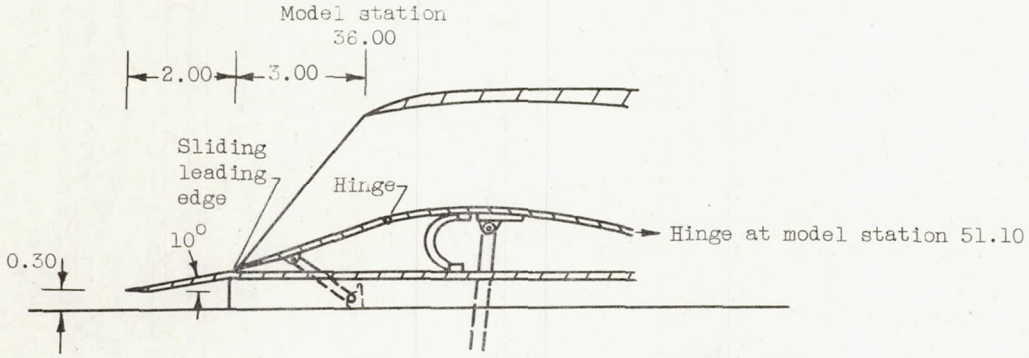

(f) Inlet 10-R-0.

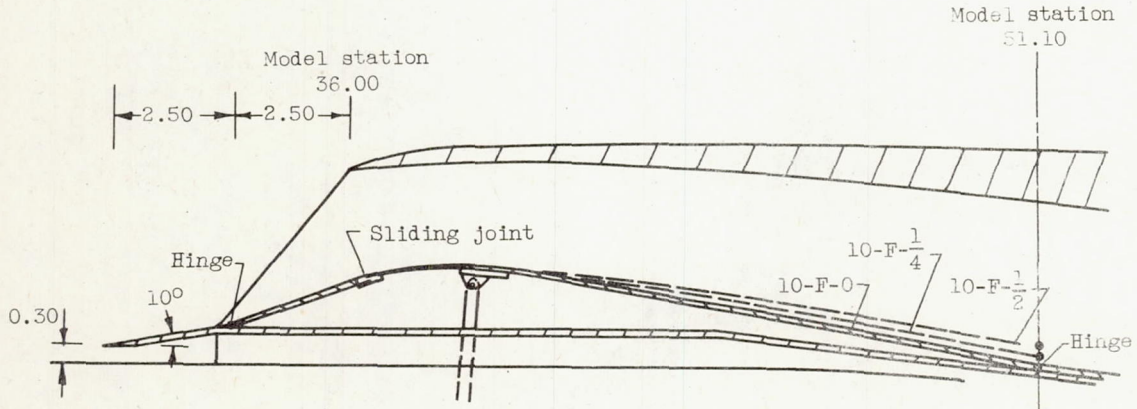

(g) Inlets 10-F-0, 10-F-$\frac{1}{4}$, and 10-F-$\frac{1}{2}$.

Figure 4. - Concluded. Detailed views of inlet configurations (all dimensions are in inches).

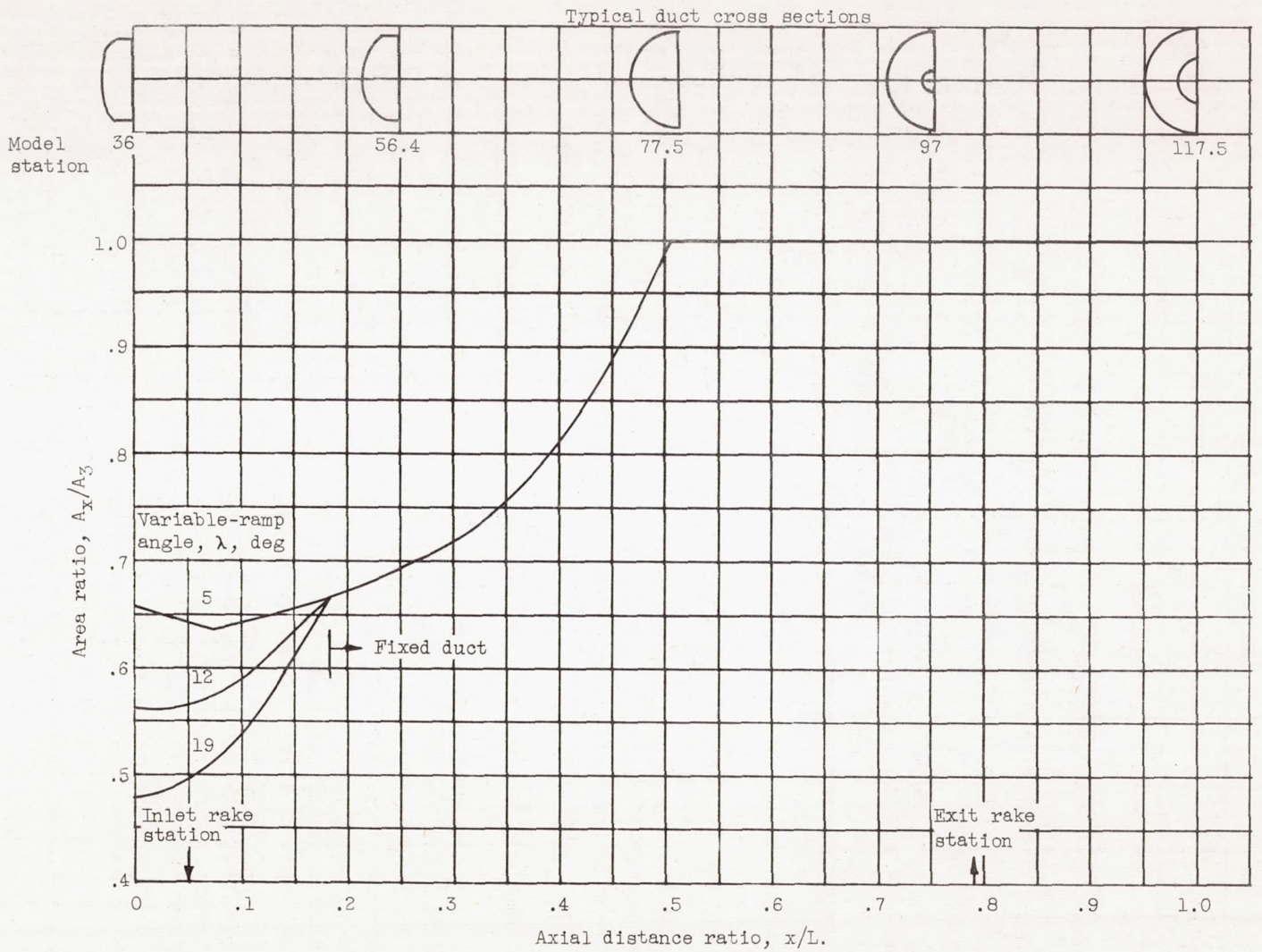

(a) Inlet 3-R-0.

Figure 5. - Subsonic diffuser area variations. L, 81.5 inches; A_3, 0.457 square feet.

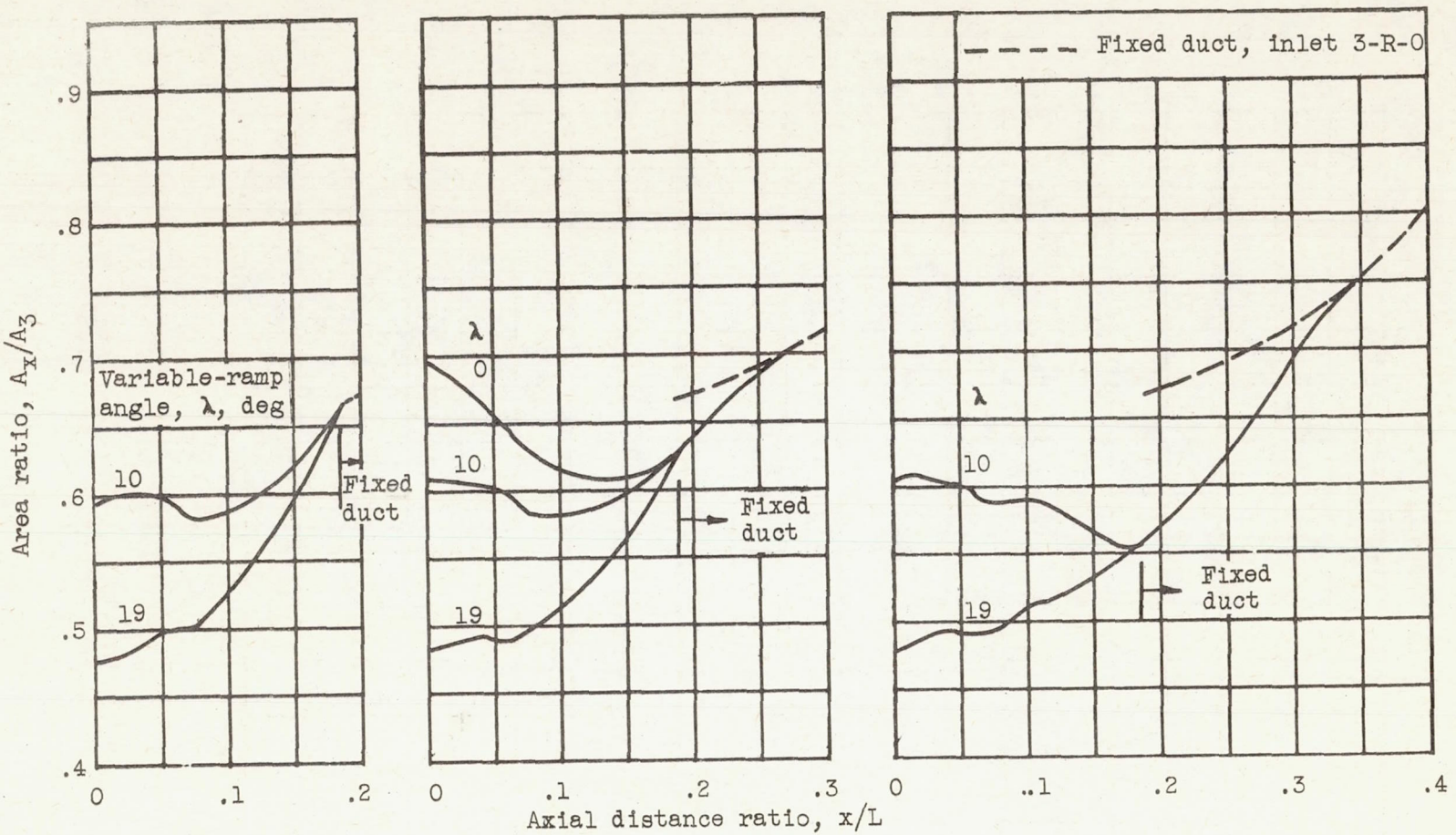

(b) Inlets 10-R-0 and 10-F-0.

(c) Inlet 10-F-1/4.

(d) Inlet 10-F-1/2.

Figure 5. - Concluded. Subsonic diffuser area variations. L, 81.5 inches; A_3, 0.457 square feet.

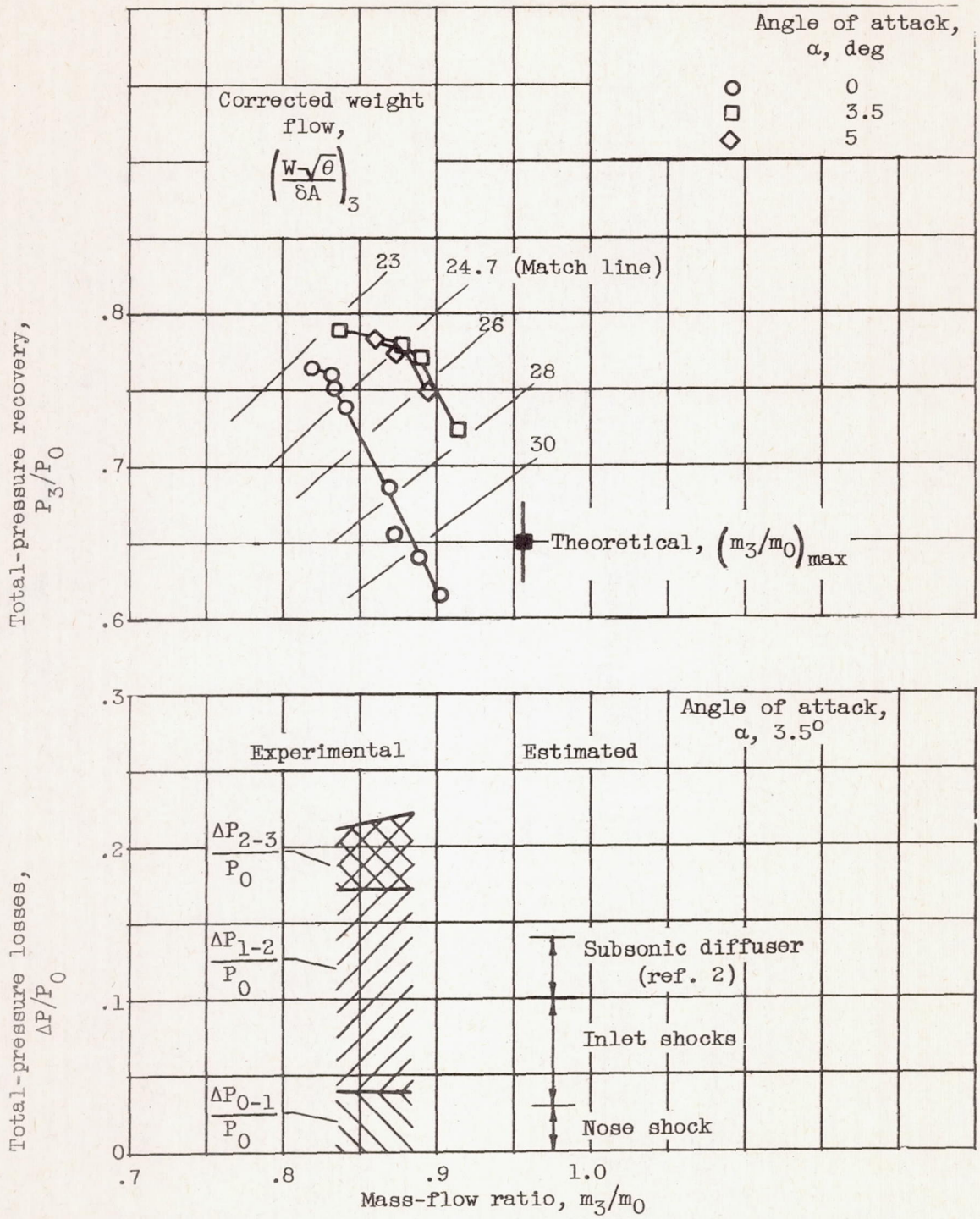

Figure 6. - Internal performance and breakdown of losses for inlet 3-R-0 at a free-stream Mach number of 2.0, and a variable-ramp angle of 19°.

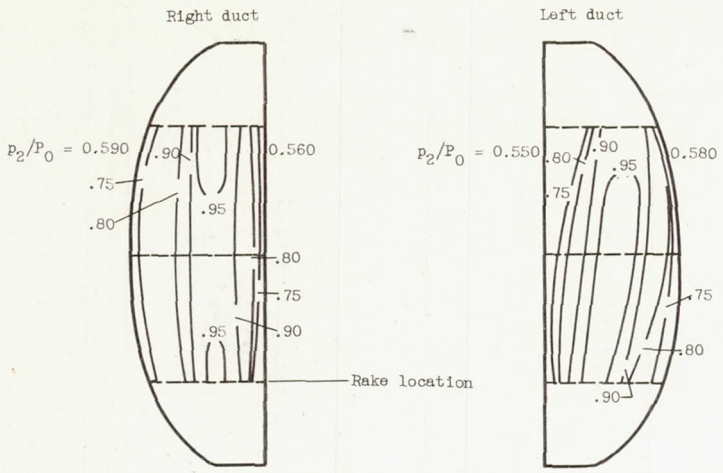

(a) Inlet 3-R-0; mass-flow ratio, 0.798.

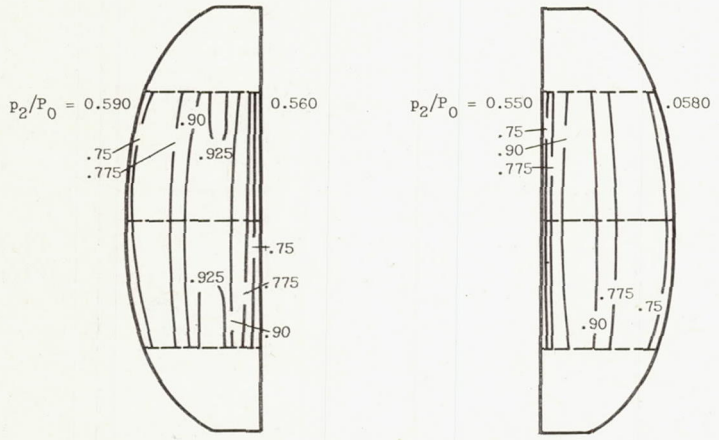

(b) Inlet 3-R-0 (boundary-layer bleed); mass-flow ratio, 0.808.

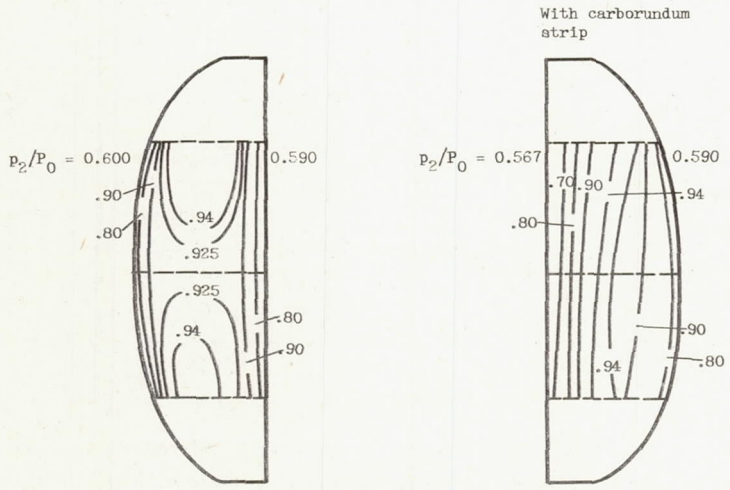

(c) Inlet 10-R-0; mass-flow ratio, 0.794.

Figure 7. - Inlet total-pressure-recovery contours for free-stream Mach number of 2.0, variable-ramp angle of 19°, and angle of attack of 3.5°.

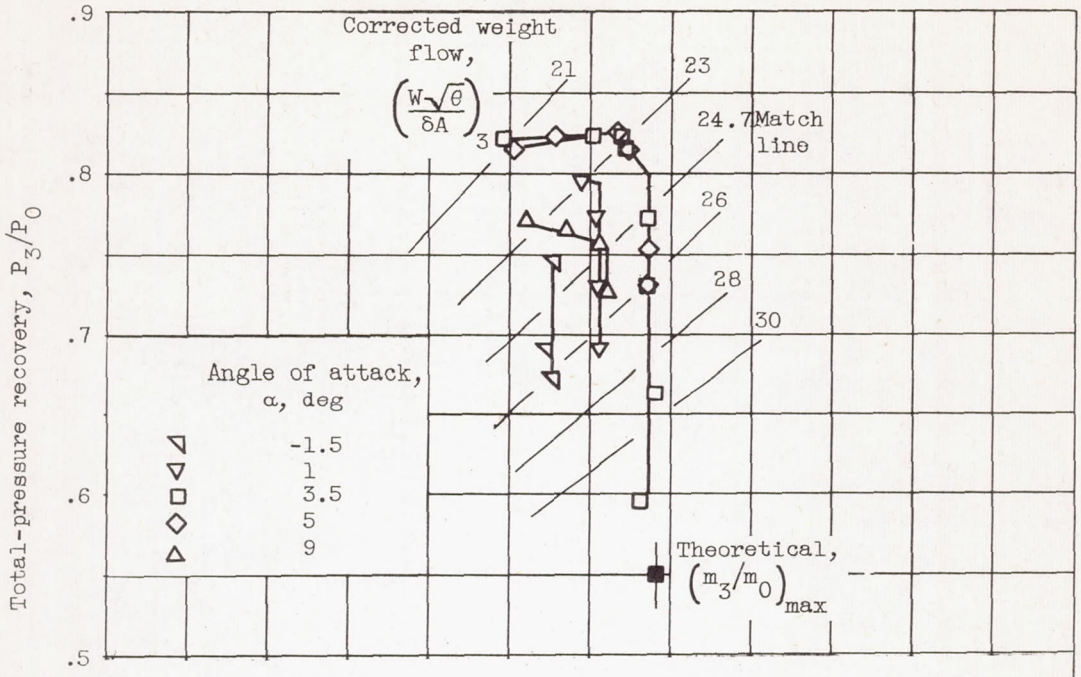

(a) Free-stream Mach number, 2.0.

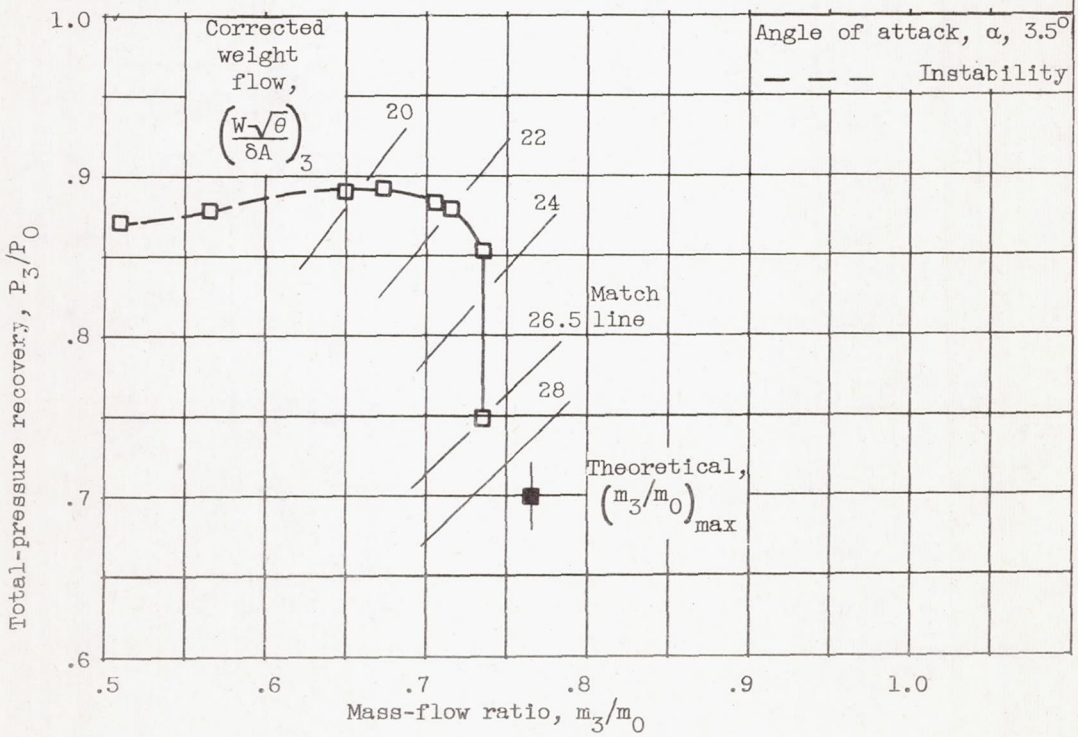

(b) Free-stream Mach number, 1.8.

Figure 8. - Internal performance of inlet 10-R-0 at variable-ramp angle of 19°.

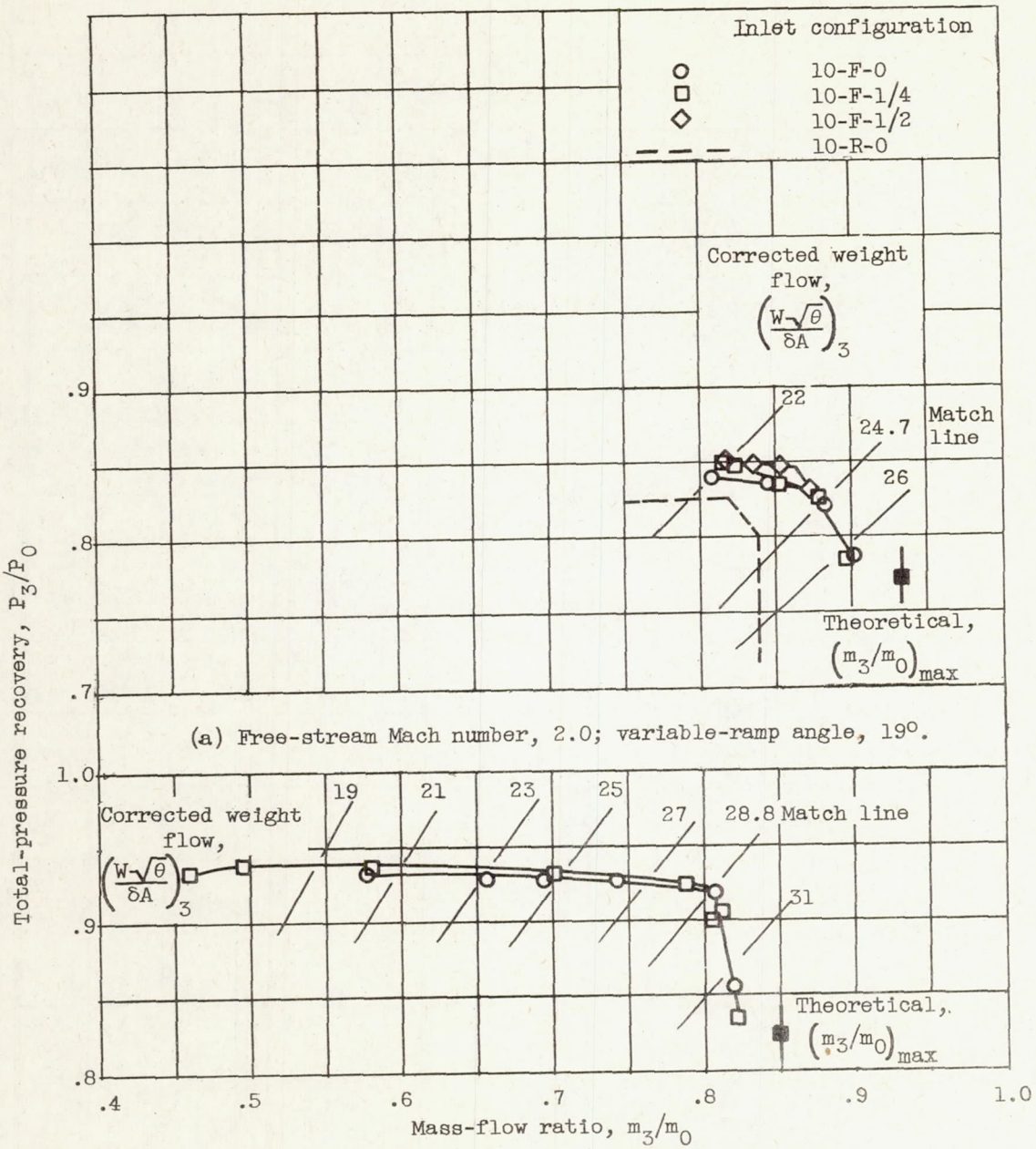

(a) Free-stream Mach number, 2.0; variable-ramp angle, 19°.

(b) Free-stream Mach number; 1.5, variable-ramp angle, 10°.

Figure 9. - Effect of diffuser area variation on inlet internal performance at angle of attack of 3.5°.

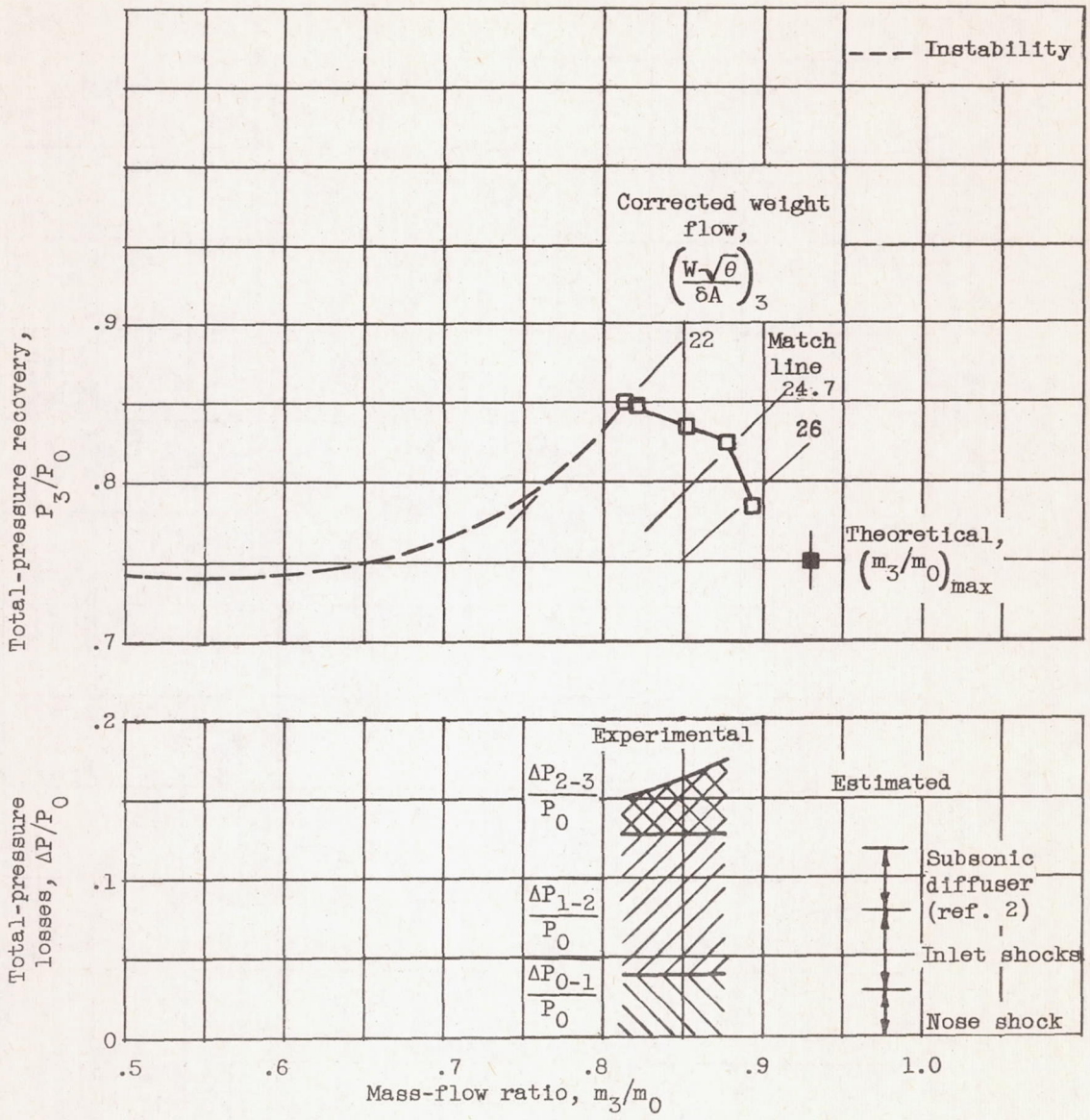

(a) Free-stream Mach number, 2.0; variable-ramp angle, 19°.

Figure 10. - Internal performance and breakdown of losses for inlet 10-F-1/4 at angle of attack of 3.5°.

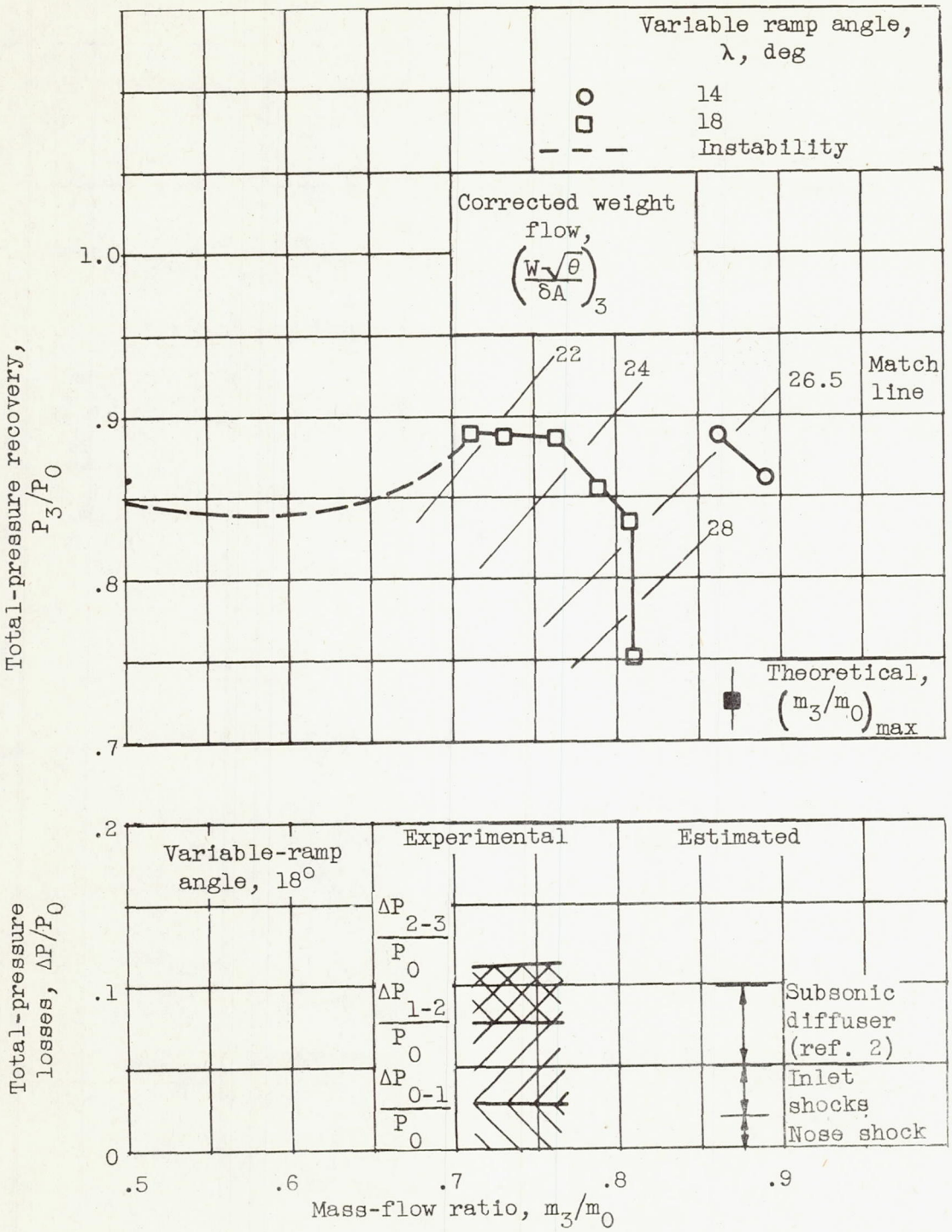

(b) Free-stream Mach number, 1.8.

Figure 10. - Continued. Internal performance and breakdown of losses for inlet 10-F-1/4 at angle of attack of 3.5°.

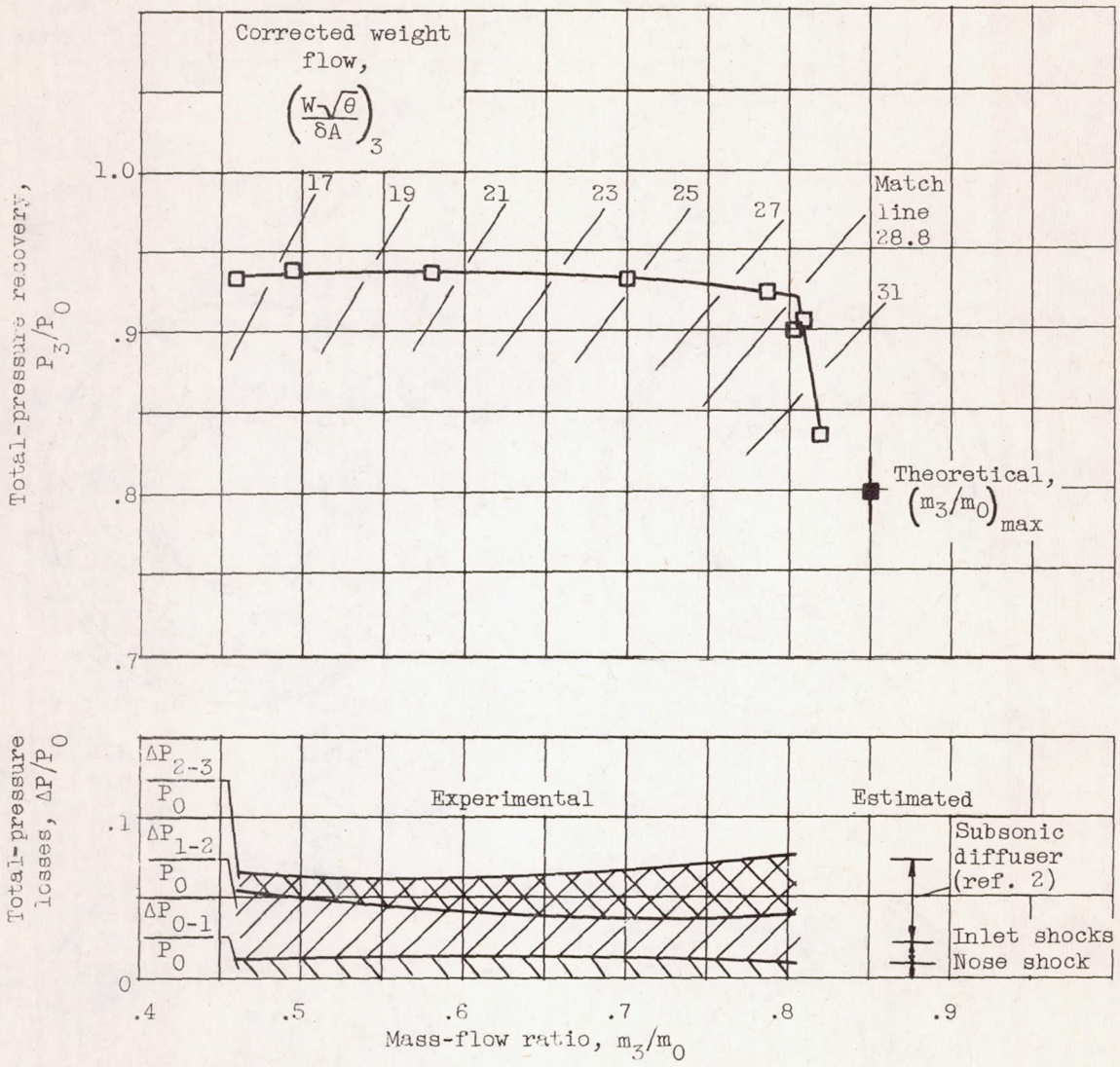

(c) Free-stream Mach number, 1.5; variable-ramp angle, 10°.

Figure 10. - Concluded. Internal performance and breakdown of losses for inlet 10-F-1/4 at angle of attack of 3.5°.

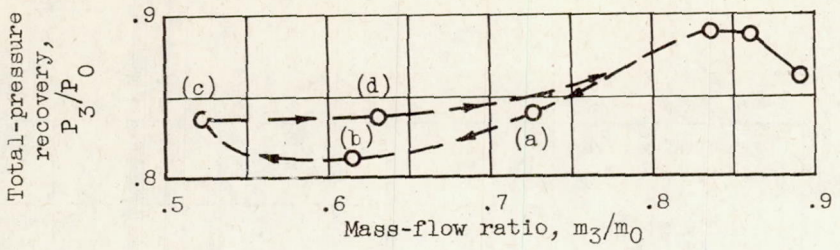

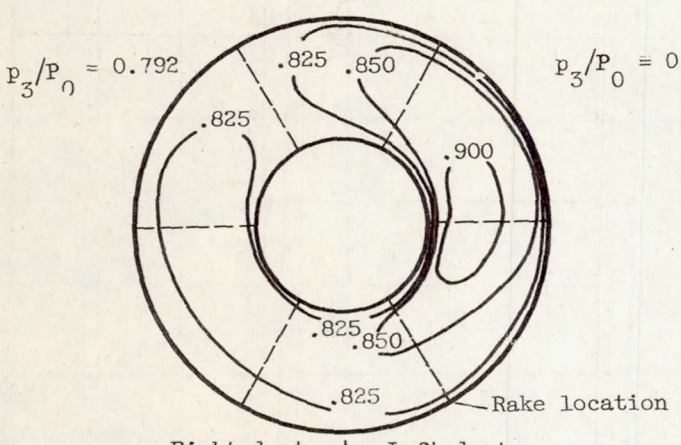

(a) Mass-flow ratio, 0.726.

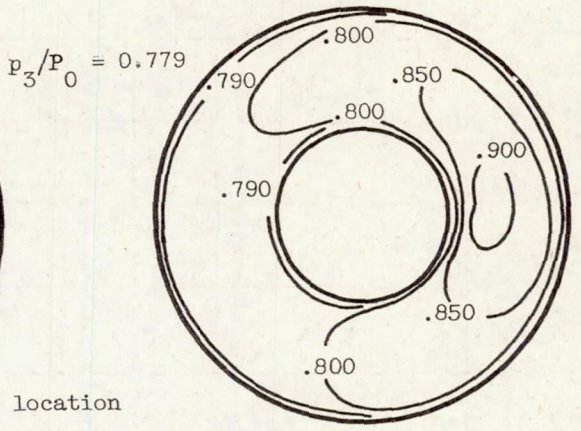

(b) Mass-flow ratio, 0.616.

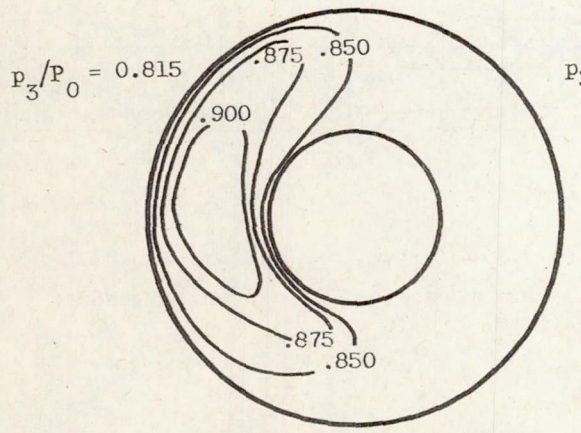

(c) Mass-flow ratio, 0.522.

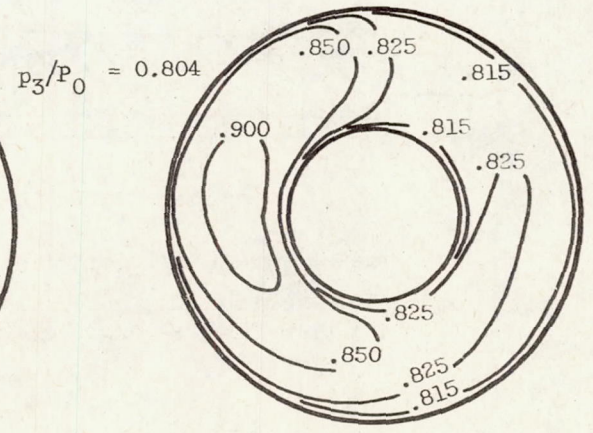

(d) Mass-flow ratio, 0.632.

Figure 11. - Internal performance and diffuser-exit contours in pulsing region for inlet 10-F-1/2 at Mach number of 1.8, angle of attack of 3.5°, and variable-ramp angle of 14°.

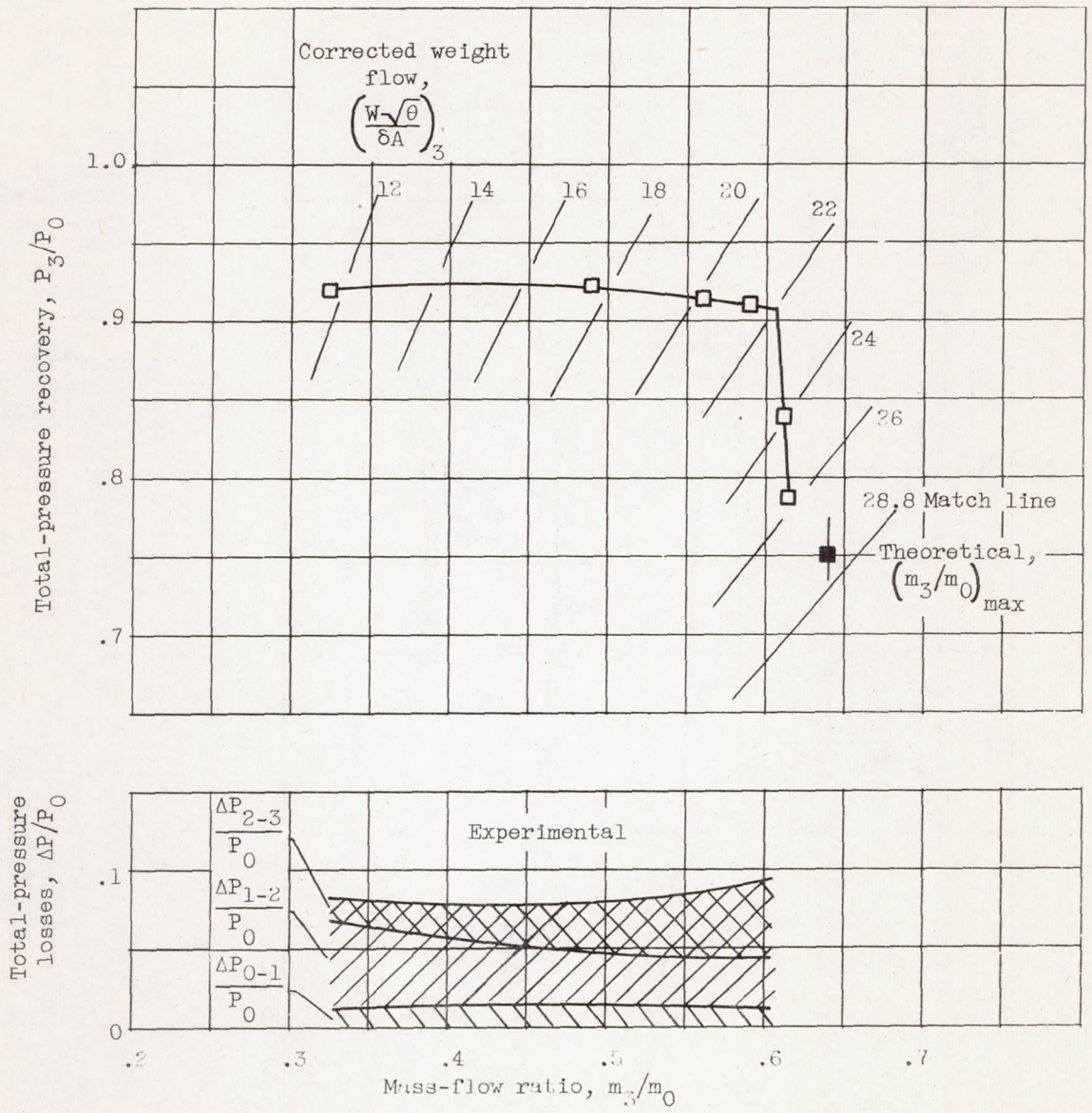

Figure 12. - Internal performance and breakdown of losses for inlet 10-R-0 at free-stream Mach number of 1.5, variable-ramp angle of 20°, and angle of attack of 3.5°.

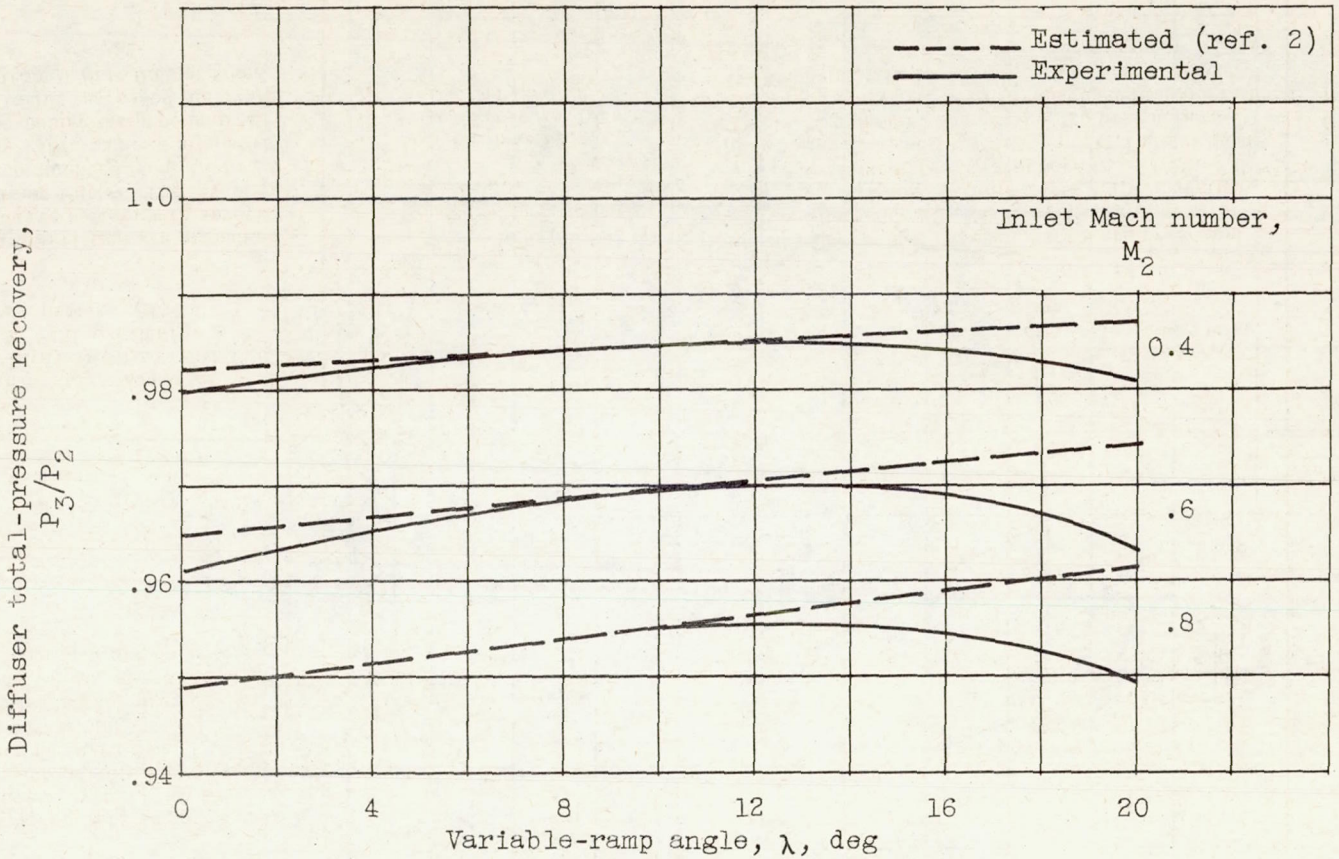

Figure 13. - Subsonic diffuser performance for inlet 10-F-1/4 at angle of attack of 3.5°.